RESEARCH ARTICLE
eISSN 2234-1757
Fish Aquat Sci. 2025;28(2):107-119
https://doi.org/10.47853/FAS.2025.e11
FAS Fisheries and Aquatic Sciences

Light-enhanced antibacterial carbon dot nanocomposite synthesized using *Sargassum horneri* and inorganic precursors

Kyung Woo Kim[1,*], Gun-Woo Oh[1], Seok-Chun Ko[1], Ji-Yul Kim[1], Chul Hwan Kim[2], Yong Min Kwon[3], Mi-Jin Yim[2], Moongeun Yoon[1], Dae-Sung Lee[1,2,3,*]

[1] *Department of Biomaterial Research, National Marine Biodiversity Institute of Korea, Seocheon 33662, Korea*
[2] *Department of Bioindustrial Strategy, National Marine Biodiversity Institute of Korea, Seocheon 33662, Korea*
[3] *Department of Biological Application & Technology, National Marine Biodiversity Institute of Korea, Seocheon 33662, Korea*

Abstract

This study aimed to introduce a novel antibacterial carbon dot-ZnO-TiO_2 nanocomposite (CDZT) synthesized from the marine alga *Sargassum horneri* and two inorganic precursors. CDZT exhibited enhanced antibacterial activity under both ultraviolet (UV) light and visible light, and its water-soluble nature suggested its potential in various industrial applications. The antibacterial activity was evaluated using disk diffusion tests under two different light conditions. CDZT showed distinct bacterial inhibition against both gram-negative and gram-positive strains, with larger inhibition zones under 365 nm UV light and 470 nm visible light, respectively. These results highlighted the promise of *S. horneri* as a valuable resource for the development of advanced antibacterial materials. The findings underscored the possibility of CDZT being a potent antibacterial agent with light-modulated activity. Since this was a proof-of-concept study, further evaluation is needed for the practical use of CDZT in antibacterial applications within the relevant industry.

Keywords: Antibacterial nanocomposite, Marine alga, Light-modulated activity, Carbon dots

Introduction

Bacterial infections, including those by antibiotic-resistant bacteria, remain significant threats to human health despite the growing medical knowledge, diagnostic techniques, as well as public interest. The menace imposes significant physical and financial burdens worldwide. At least 700,000 deaths per year occur globally, and the number is expected to reach 10 million

Received: Jul 2, 2024 **Revised:** Sep 27, 2024 **Accepted:** Oct 7, 2024
***Corresponding author:** Kyung Woo Kim
Department of Biomaterial Research, National Marine Biodiversity Institute of Korea, Seocheon 33662, Korea
Tel: +82-41-950-0936 , **Fax:** +82-41-950-0931, **E-mail:** kimkw79@mabik.re.kr
***Corresponding author:** Dae-Sung Lee
Department of Bioindustrial strategy, National Marine Biodiversity Institute of Korea, Seocheon 33662, Korea
Tel: +82-41-950-0900 , **E-mail:** daesung@mabik.re.kr

deaths annually by 2050. Antibacterial agents are, therefore, essential for human beings (Cheeseman et al., 2020; Correa et al., 2020; Huang et al., 2020; Ribeiro et al., 2022), and novel antibacterial materials are being steadily developed. In 2021, the World Health Organization (WHO) published a report on the clinical and preclinical developments regarding antibacterial agents, and examined the urgent need for new antibacterial agents. Sincere efforts are required to develop antibacterial materials, regardless of the industry or academia. Nanotechnology delivers innovative medical achievements and solutions for progress in the field of human healthcare (Sindhwani & Chan, 2021). Antibacterial nanomaterials form a rapidly developing branch of nanotechnology. To improve the antibacterial performance of nanomaterials, their surface functionalization should be considered using materials such as cationic polymers, metals, and antifouling agents. Inorganic antibacterial nanoaparticles are mostly based on metals or metal oxides. They contain single metals, such as gold (Au), bismuth (Bi), copper (Cu), selenium (Se), and silver (Ag), or metal oxides, such as aluminum oxide (Al_2O_3), calcium oxide (CaO), ferric oxide (Fe_2O_3), magnesium oxide (MgO), or titanium dioxide (TiO_2), zinc oxide (ZnO) (Hochvaldová et al., 2022). Among these, ZnO and TiO_2 are well-known nontoxic biocidal and multipurpose nanomaterials, and their safety and functional benefits have been approved by the USA. Food and Drug Administration (FDA) for only sunscreen or cosmetic products for ultraviolet (UV)-protection (Faure et al., 2013). ZnO and TiO_2 have been used as additives in several industries. ZnO is a water-insoluble inorganic white powder used in cosmetics, food, lubricants, rubbers, paints, pigments, adhesives, plastics, ceramics, glasses, cement, and batteries (Subhan et al., 2022). TiO_2 is a white-colored inorganic powder that is insoluble in water and is used in paints, printing ink, synthetic fibers, plastics, rubbers, food, cosmetics, and electric components (Haider et al., 2019). In particular, ZnO and TiO_2 are considered to be good photocatalysts owing to their low toxicity, low cost, and excellent chemical stability in the semiconductor industry (Pei et al., 2016; Wang et al., 2022). However, despite the good catalytic properties, they have some drawbacks; for example, the large band gaps of ZnO and TiO2 (3.37 eV and 3.2 eV, respectively), the fast electron-hole recombination due to which they can only be excited under UV irradiation in a specific wavelength range (< 400 nm), the deficit of visible light absorption, and limited use of natural sunlight (Cho et al., 2020; Jia et al., 2018; Pei et al., 2016; Wang et al., 2022). In addition, their wide bandgap can act as a limiting factor for their antibacterial properties. Interestingly, the antibacterial activities of ZnO and TiO_2 are affected by light. Although ZnO shows antibacterial activity in the dark, its antibacterial actions are activated only by UV light, which is followed by the release of reactive oxygen species (Azizi-Lalabadi et al., 2019; Mendes et al., 2022). Nanocomposites have emerged as powerful tools for enhancing the properties of base materials and introducing new functionalities through combination of different nanomaterials. Therefore, several studies have attempted to produce novel nanocomposites by combining two versatile materials (Aga et al., 2022; Feng et al., 2021; Shameem et al., 2021; Singh et al., 2021). By fabricating a nanocomposite of ZnO and TiO_2, the photocatalytic response could be boosted to prolong charge separation, reduce recombination rates, and activate responses to a wide range of light (Shaker et al., 2020; Upadhyay et al., 2019). Our previous study had shown the antimicrobial activity of a carbon dot-ZnO nanocomposite based on the marine alga *Sargassum horneri* against bacteria and fungi, regardless of UV light irradiation. In that study, the nanocomposite exhibited an improved antibacterial effect upon UV irradiation in a specific bacterial group; however, this was only obtained in the range of 365 nm UV light (Kim et al., 2022a). Carbon dots (CDs) are novel and promising nanomaterials with applications in various fields (Gayen et al., 2019; Liu et al., 2020; Nocito et al., 2021). Antimicrobial activity, low cytotoxicity, biocompatibility, cellular uptake affinity, and antiviral activity have been reported as the characteristics of CDs (Ghirardello et al., 2021; Nocito et al., 2022; Wu et al., 2022; Zhao et al., 2023). CDs, which typically have diameters less than 10 nm, are commonly synthesized using either top-down or bottom-up methods. Their green and eco-friendly synthesis from biowastes and natural materials makes them highly desirable (Chahal et al., 2021; Jing et al., 2023; Kanwal et al., 2022). CDs offer a promising platform for various applications including bioimaging, biosensing, photocatalysis, optoelectronics, energy conversion, UV degradation, and reinforcement. We hypothesized that the incorporation of CDs could significantly enhance the performance of nanocomposites, offering new avenues for the fabrication of high-performance materials (de Oliveira et al., 2020; He et al., 2024).

The current report aimed to propose a novel carbon dot-ZnO-TiO_2 nanocomposite (CDZT) based on the marine alga *S. horneri* and two inorganic precursors, namely zinc acetate dehydrate and titanium (IV) isopropoxide. *S. horneri*, a type of brown algae, is widely distributed along the coasts of Korea, Japan, and China. Its invasion, which washes up from the ocean

https://doi.org/10.47853/FAS.2025.e11

and causes various problems when it reaches the coast, has started again this year. This issue has been ongoing for 10 years since it was first reported on the coasts of Jeju and Jeonnam provinces in 2015. Particularly, *S. horneri* has air sacs that allow it to travel far with ocean currents. Even while floating, it can continue to grow under the proper conditions, forming large piles. When *S. horneri* accumulates on the coast, it not only spoils the scenery but also produces toxic gases such as hydrogen sulfide and ammonia as it decays, which are harmful to health. Its tough stems are difficult to split and can entangle in ship screws, causing accidents or malfunctions. Since it is hardly possible to eliminate its incoming, research on the utilization of *S. horneri* is highly necessary. Leveraging the benefit of synthesizing CDs from biowastes, this research focused on developing an antibacterial nanocomposite using *S. horneri*. Here, *S. horneri* was utilized as the initial material for the fabrication of CDs and as a multi-precursor for the organic synthesis of ZnO and TiO_2. The antibacterial activity of the CDZT was demonstrated not only under UV irradiation in the UV-A range, but also under visible light at 450 nm. Since the nanocomposite was soluble in water after fabrication, its industrial applications would be highly feasible.

Materials and Methods

Materials

From Byeonsan Beach area in Buan-gun, Jeollabuk-do (35°40'51.8"N, 126°31'50.9"E), a bundle of *S. horneri* was collected manually. Sigma-Aldrich (St. Louis, MO, USA) supplied the zinc acetate dihydrate, titanium (IV) isopropoxide (TTIP), and absolute ethanol (EtOH). Paper discs (diameter = 8 mm, thickness = 0.7 mm) were obtained from Advantec (Tokyo, Japan). UltraPure™ DNase/RNase-free distilled water, BD Difco™ Luria-Bertani (LB) broth, BD Difco™ agar, and Minisart® NML syringe filters were purchased from Thermo Fisher Scientific (Waltham, MA, USA). Escherichia coli (KCTC1682), Bacillus cereus (KCTC1682), *Salmonella typhimurium* (KCTC1925), and *Staphylococcus aureus* (KCTC1927) were obtained from the Korean Collection for Type Cultures (KCTC) and American Type Culture Collection (ATCC).

Synthesis of carbon dot-ZnO-TiO_2 nanocomposite (CDZT) and collection of TiO_2 powders

CDZT was fabricated by simply utilizing *S. horneri* with two inorganic precursors in a single-pot hydrothermal reaction. Two grams of *S. horneri* were properly cleaned under running water to get rid of any remaining salt and sand, and were then dried at 40℃. The cleaned and dried *S. horneri* was placed in a mini-pulverizer and crushed into fine powder. First, 1 g of the as-prepared *S. horneri* powder was mixed with a TTIP solution prepared by dissolving 1 mL of TTIP in 9 mL of EtOH. Ten milliliters of ultrapure water and 5 mL of EtOH were then added to the *S. horneri*-TTIP mixture solution. Zinc acetate dihydrate (0.5 g) was then added to the mixture, which was placed in a hydrothermal autoclave (TEFIC Biotech, Xi'an, China). The reactor was placed at 180℃ for 6 h and cooled to 25℃ thereafter. The fabricated CDZT solution was centrifuged using a Frontier™ 5718R centrifuge with Frontier™ 5,000 rotor (Ohaus, Parsippany, NJ, USA) at 4,400 rcf for 30 min at 24℃. The supernatant was filtered using a syringe filter with a 0.22-μm porous membrane. The final CDZT solution (pH 6–6.5) was stored in the refrigerator at 4℃ until use. The precipitates remaining after filtration were collected and washed thrice with EtOH and ultrapure water. The washed precipitates were calcined at 400℃ for 3 h to obtain a white-colored TiO_2 powder (Fig. 1B).

Fabrication of carbon dots and carbon dot-TiO_2 nanocomposite

To investigate the morphology of CDZT, two different nanomaterials, such as carbon dot alone (CDA) and carbon dot-TiO_2 nanocomposite (CDT), were synthesized using *S. horneri* through a hydrothermal reaction. Pulverized *S. horneri* was prepared in the same way as described in the preceding section. To fabricate CDA, 2 g of *S. horneri* were mixed with 5 mL of EtOH and sonicated in a water bath for 30 min. After adding 15 mL of ultrapure water, hydrothermal treatment was performed at 180℃ for 6 h. The supernatant was separated by centrifugation at 4,400 rcf for 30 min at 24℃, and the final CDA solution was obtained through a 0.22-μm porous filter. To prepare the CDT solution, 2 g of *S. horneri* fine powders were taken in 19 mL of EtOH:ultrapure water (5 mL:14 mL) mixed solution. The mixed solution was subjected to ultrasound treatment for 30 min in a water bath, and then 1 mL of TTIP was added to the solution, followed by thorough mixing. Hydrothermal treatment of the mixed solution was conducted at 180℃ for 6 h. The final CDT solution was obtained by filtering it through a 0.22-μm porous membrane.

Investigation of the morphological properties of carbon dot-ZnO-TiO_2 nanocomposite (CDZT)

Using a JEM-ARM200F microscope operated at 80 kV (JEOL,

Tokyo, Japan), photos of the CDZT and TiO_2 were collected, and the analytical data of energy dispersive X-ray spectroscopy (EDS) were obtained concurrently. The diluted CDZT solution, mixed with ultrapure water, was applied to a transmission electron microscopy (TEM) grid with a Formvar film coated with carbon (Ted Pella, Redding, CA, USA) and allowed to air-dry before being used to analyze the TEM images. The particle sizes were measured using ImageJ software based on the TEM images, and particle size distributions were calculated using the Gaussian distribution of origin software version 8.6 (OriginLab, Northampton, MA, USA).

Fourier-transform infrared (FT-IR) spectroscopy and X-ray photoelectron spectroscopy (XPS) for CDZT, CDT, and CDA were performed using a Frontier MIR/FIR spectrometer from 400 cm^{-1} to 4,000 cm^{-1} (PerkinElmer, Waltham, MA, USA) by the ATR method and a PHI5000 VersaProbe III photoelectron spectrometer (Ulvac-Phi, Chigasaki, Japan) including an Al Kα_radiation source (hv = 1,486.6 eV), respectively. Prior to performing the FT-IR and XPS analyses, the CDZT solution was freeze-dried using a FreeZone drying machine (Labconco, Kansas City, MO, USA) at –80℃ for 3 days. FT-IR and XPS were performed on both the lyophilized CDZT and as-calcined TiO_2 powders.

Investigation of the optical characteristics of carbon dot-ZnO-TiO_2 nanocomposite (CDZT)

Photoluminescence (PL) spectra were recorded using a FluoroMax-4 spectrometer (HORIBA, Kyoto, Japan) over the wavelength range of 270 nm to 700 nm, with excitation wavelengths varying from 250 nm to 550 nm in 10-nm increments. The UV–vis absorption spectra were acquired from 220 nm to 800 nm using a BioSpectrometer® basic (Eppendorf, Hamburg, Germany). Fluorescent photo-images of CDZT were captured using a home digital camera (EOS M6, Canon, Tokyo, Japan) under LED light (12 W, 21 mW/cm^2) at 470 nm (BluPAD; BioD, Gwangmyeong, Korea) or UV light (6 W, 0.6 mW/cm^2) at 365 nm (VL-6. LC; Vilber, Collégien, France).

Test for antibacterial activity

First, two strains each of gram-positive bacteria (*B. cereus* and *S. aureus*) and gram-negative bacteria (*E. coli* and *S. typhimurium*) were cultured in 20 mL of LB media at 37℃ overnight to demonstrate the antibacterial activities of as-fabricated CDZT nanocomposite. Colony-forming units (CFUs) were measured using a QUANTOM Tx™ microbial cell counter (Logos Biosystems, Anyang, Korea), following which all bacterial strains were adjusted to 1×10^7 CFU/mL. Two hundred microliters of each bacterial broth were spread over LB-agar plates, 30 μL of as-prepared CDZT solution were adjusted to paper discs (diameter = 8 mm, thickness = 0.7 mm), and then appropriately placed on the LB-agar plates. To examine the light-enhanced antibacterial effects with and without UV and visible light, two plates were prepared for each strain. Each plate was incubated overnight at 37℃, either with or without both UV light at 365 nm (6 W, 0.6 mW/cm^2) and LED light at 470 nm (12 W, 21 mW/cm^2). Antibacterial activities of the CDZT nanocomposite against the four bacteria were determined by measuring the size of the inhibition zone of paper disks on the plates and comparing the differences between no light and either of UV light at 365 nm and visible light at 470 nm. Size of the inhibition zones was measured using a digital caliper (CD-8" ASX; Mitutoyo, Kawasaki, Japan). A comparative antibacterial experiment using CDT was performed as described above, and all experimental results were confirmed in triplicate.

Results and Discussion

Morphological properties of carbon dot-ZnO-TiO_2 nanocomposite (CDZT)

A comprehensive structural analysis and size distribution calculation of the CDZT nanocomposite was conducted using high-resolution transmission electron microscopy (HR-TEM; Figs. 1 and 2). Particle sizes of the CDZT nanocomposite (derived from the supernatant) and the pure titanium dioxide (TiO_2) nanoparticles (obtained from precipitates) after synthesis via hydrothermal reaction and calcination at 400℃ for 3 h were examined separately (Figs. 3 and 4). Particle size distribution was estimated using TEM images processed with origin 8 software. Most of the measured particle sizes were within the range of 6–8 nm. However, the CDZT supernatant exhibited a more diverse size distribution than its precipitates. The supernatant, which had only been filtered through a 0.22-μm-pore membrane, was a complex mixture, whereas the precipitate, being pure TiO_2 that had undergone a calcination process, was considered to have a more uniform size distribution. Furthermore, their atomic concentrations were investigated using EDS concurrently with HR-TEM imaging. The supernatant of CDZT was found to be composed of carbon, oxygen, titanium, and zinc, whereas the precipitate consisted of carbon (C), oxygen (O), and titanium (Ti; Figs. 3 and 4). The detailed analysis

https://doi.org/10.47853/FAS.2025.e11

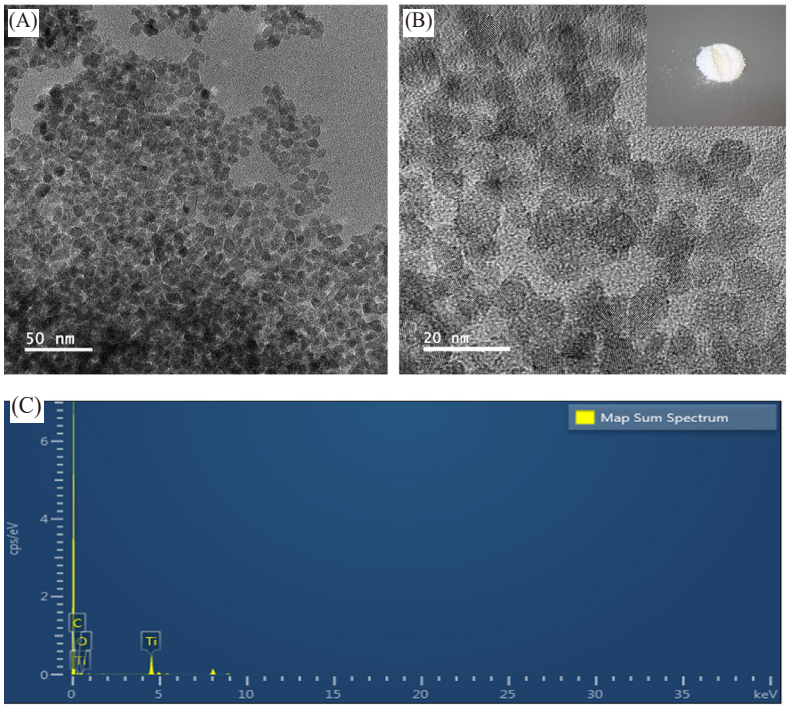

Fig. 1. Morphological analysis and elemental classification using the TEM/EDS. (A and B) Transmission electron microscopy (TEM) images of pure TiO_2 nanoparticles after calcination and (C) the energy dispersive X-ray spectroscopy (EDS) mapping of a selected region of TEM image.

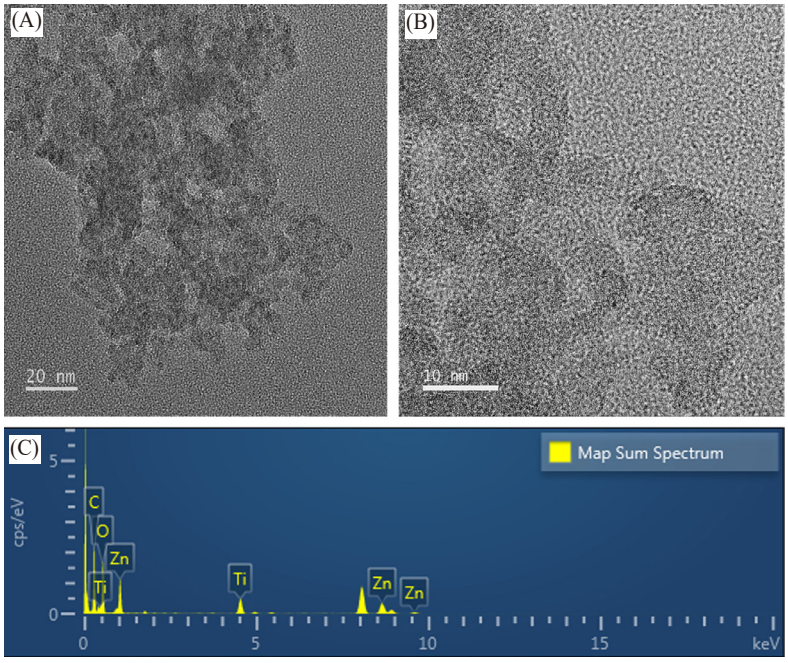

Fig. 2. Morphological analysis and elemental classification using the TEM/EDS. (A and B) Transmission electron microscopy (TEM) images of carbon dot-ZnO-TiO_2 nanocomposite (CDZT) from supernatant and (C) the energy dispersive X-ray spectroscopy (EDS) mapping of a selected region of TEM image.

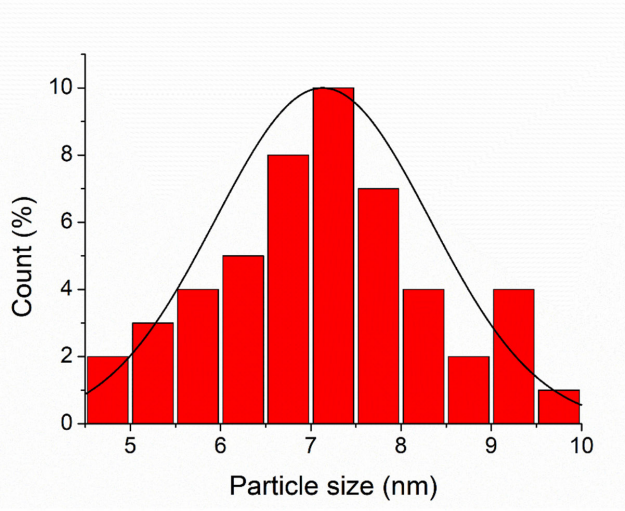

Element	Wt%	Wt% Sigma	Atomic %
C	54.74	0.61	70.70
O	24.28	0.48	23.54
Ti	9.09	0.22	2.94
Zn	11.89	0.30	2.82
Total:	100.00		100.00

Fig. 3. Size distribution of carbon dot-ZnO-TiO_2 nanocomposite (CDZT) and its chemical composition from energy dispersive X-ray spectroscopy (EDS) analysis.

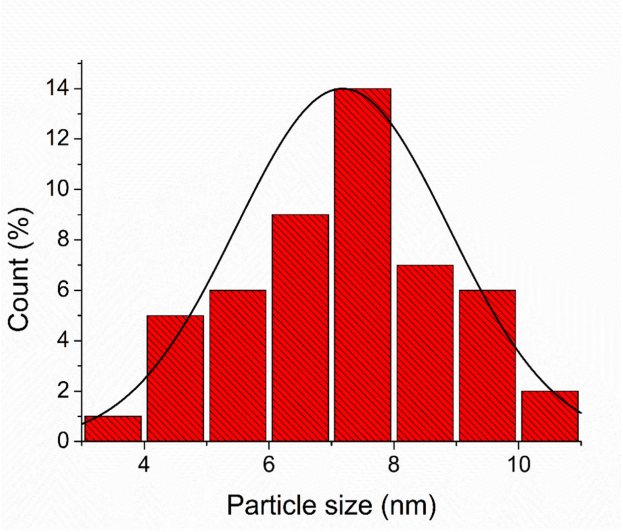

Element	Wt%	Wt% Sigma	Atomic %
C	15.05	0.91	37.20
O	8.22	0.76	15.24
Ti	76.73	1.04	47.55
Total:	100.00		100.00

Fig. 4. Size distribution of pure TiO_2 and its chemical composition from energy dispersive X-ray spectroscopy (EDS) analysis.

provided precious perspective into the structural characteristics and atomic composition of CDZT nanocomposites, contributing to our understanding of their potential applications and performance.

To comprehensively evaluate the morphological characteristics of CDZT nanocomposites, comparative samples of CDA and CDT were prepared. The comparative approach allowed for a more nuanced understanding of the unique properties of CDZT, since it provided a benchmark against which CDZT could be evaluated. The spectra from FT-IR and XPS were obtained for all three samples, namely CDZT, CDA, and CDT. The spectroscopic techniques provided valuable insights into the chemical bonding, functional groups, and electronic states of samples, thereby shedding light on their structural and chemical characteristics. The FT-IR spectra of the samples were recorded simultaneously to allow a direct comparison of the vibrational frequencies, which could reveal information about the types of bonds present in the samples. Fig. 5 compares the FT-IR spectra of CDA, CDT, and CDZT. By analyzing the spectra, we gained insight into the similarities and differences in the chemical structures of these nanocomposites. This approach,

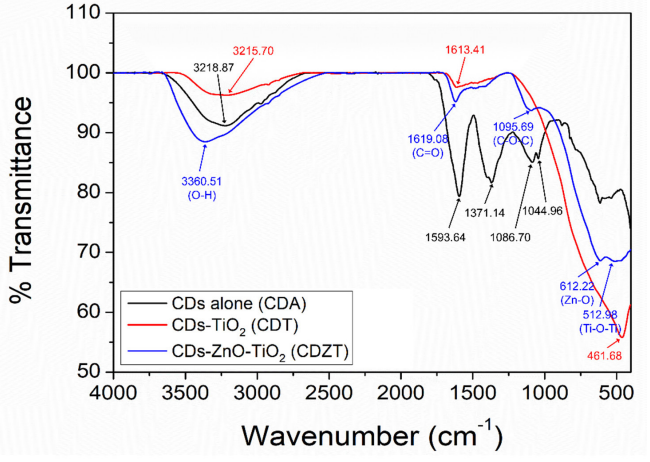

Fig. 5. Comparison of the Fourier-transform infrared (FT-IR) spectra of carbon dot alone (CDA), carbon dot–TiO_2 nanocomposite (CDT), and carbon dot-ZnO-TiO_2 nanocomposite (CDZT).

https://doi.org/10.47853/FAS.2025.e11

which combined morphological investigation with spectroscopic analysis, allowed us to delve deeper into the unique properties of CDZT nanocomposites. This also set the stage for further studies aimed at optimizing the properties of CDZT for various applications. The specific findings from the FTIR and XPS spectra are discussed below.

The CDZT spectrum had stretching vibration peaks of O-H at 3,360.51 cm^{-1}, C = C at 1,619.09 cm^{-1}, C-O at 1,095.69 cm^{-1}, Zn-O at 612.22 cm^{-1}, and Ti-O at 512.98 cm^{-1}. The CDT spectrum showed each vibration frequency for O-H stretching at 3,215.70 cm^{-1}, C = O stretching at 1,613.41, and Ti-O stretching at 461.68 cm^{-1}. In comparison with the CDZT and CDT spectra, the spectrum of CDA showed diverse peaks at 3,218.87 cm^{-1}, 1,593.64 cm^{-1}, 1,371.14 cm^{-1}, 1,086.70 cm^{-1}, and 1,044.96 cm^{-1} corresponding to O-H stretching, C = O stretching, C-H bending, C-N stretching, and C-O stretching, respectively. CDZT showed two peaks below 1,000 cm^{-1}, attributed to Zn-O and Ti-O stretching bands, whereas CDT showed a plain peak corresponding only to the Ti-O stretching vibration. In addition, a blueshift or redshift occurred in certain bands of O-H and C = O due to conformational differences in the formation of the nanocomposite.

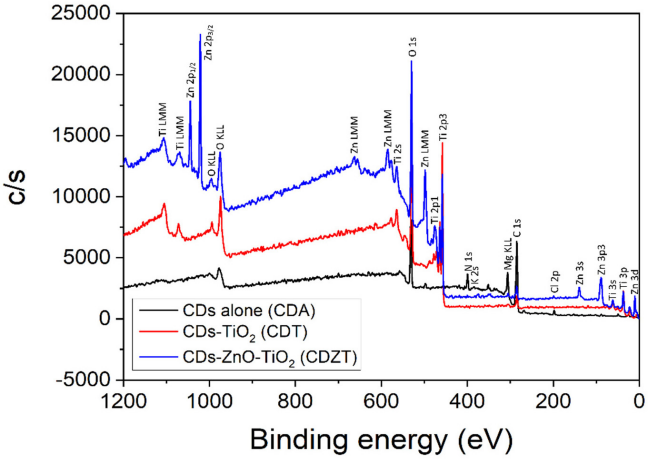

Sample	C	N	O	Zn	Ti
CDs alone (CDA)	68.79	8.70	22.50	-	-
CDs-TiO_2 (CDT)	12.94	0.57	66.93	-	19.56
CDs-ZnO-TiO_2 (CDZT)	8.93	0.50	55.85	23.02	11.70

Fig. 6. Comparison of X-ray photoelectron spectroscopy (XPS) survey spectra and atomic concentrations of carbon dot alone (CDA), carbon dot–TiO_2 nanocomposite (CDT), and carbon dot-ZnO-TiO_2 nanocomposite (CDZT).

To further verify the FTIR results, XPS analysis was performed on CDZT, CDT, and CDA (Fig. 6). In case of the CDZT composite, the presence of C (C 1s; 286.28 eV), O (O 1s; 531.36 eV), Zn (Zn 3d; 11.46 eV, Zn 3p; 89.25 eV, Zn 3s; 139.97 eV, Zn 2p3/2; 1,021.51 eV, Zn 2p1/2; 1,045.10 eV), and Ti (Ti 3p; 37.79 eV, Ti 3s; 60.71 eV, Ti 2p3; 458.05 eV, Ti 2p1; 476.73 eV, Ti 2s; 565.25 eV) elements was revealed, whereas C (285.79 eV), O (530.14 eV), and Ti (Ti 3p; 37.06 eV, Ti 3s; 59.74 eV, Ti 2p3; 457.47 eV, Ti 2p1; 473.08 eV, Ti 2s; 564.28 eV) elements (except Zn) were found present in CDT. Additionally, the presence of C (284.82 eV), N (400.41 eV), and O (532.82 eV) without Zn and Ti was confirmed in CDA. Similar to the FT-IR results, peaks for both Zn and Ti were confirmed in CDZT, but only Ti or neither could be validated in CDT or CDA, respectively. The atomic percentages (at%) of CDZT are shown in Fig. 3 as C = 8.93%, N = 0.50%, O = 55.85%, Ti = 11.70%, and Zn = 23.02%. However, those of CDT and CDA were C = 12.94% and 68.79%, N = 0.57% and 8.70%, O = 55.85% and 22.50%, and Ti = 19.56% and 0%, respectively.

High-resolution XPS spectra of CDZT with C 1s, O 1s, Zn 2p, and Ti 2p were obtained, as shown in Fig. 7. The N 1s peak is not shown in the figure, since its intensity was too low for predicting the atomic environment. In the C 1s spectrum of CDZT, the three peaks corresponded to $C(sp^2)$ – $C(sp^3)$ / $C(sp^2)$ = $C(sp^2)$ at 284.36 eV, $C(sp^3)$ – O at 285.49 eV, and carbonyl C = O at 288.49 eV. The O 1s spectrum exhibited two peaks at 529.61 eV and 531.36 eV that were associated with Zn-O/Ti-O and C-OH/C-O-C, respectively. The deconvolution of Zn 2p showed clearly identified symmetrical peaks at 1,021.41 eV and 1,044.47 eV corresponding to the Zn^{2+} oxidation state of Zn $2p_{3/2}$ and Zn $2p_{1/2}$. Difference between the binding energies of Zn $2p_{3/2}$ and Zn $2p_{1/2}$ was 23.06 eV, being similar to the standard value of 23 eV (Wang et al., 2023). In addition, the double Ti 2p peaks at 458.38 eV and 464.13 eV were assigned to Ti $2p_{3/2}$ and Ti $2p_{1/2}$. The values almost matched the well-known binding energy locations at 458.6–459.5 eV and 463.0–464.8 eV for TiO_2 (Krishnan et al., 2017).

Optical characteristics of carbon dot-ZnO-TiO_2 nanocomposite (CDZT)

The CDZT solution synthesized through a one-pot hydrothermal process exhibited a dark brown color (Fig. 8A). Photographic images of the fluorescent CDZT were obtained under both UV and visible light conditions (Fig. 8B and 8C). Interestingly, despite the formation of a nanocomposite with ZnO and

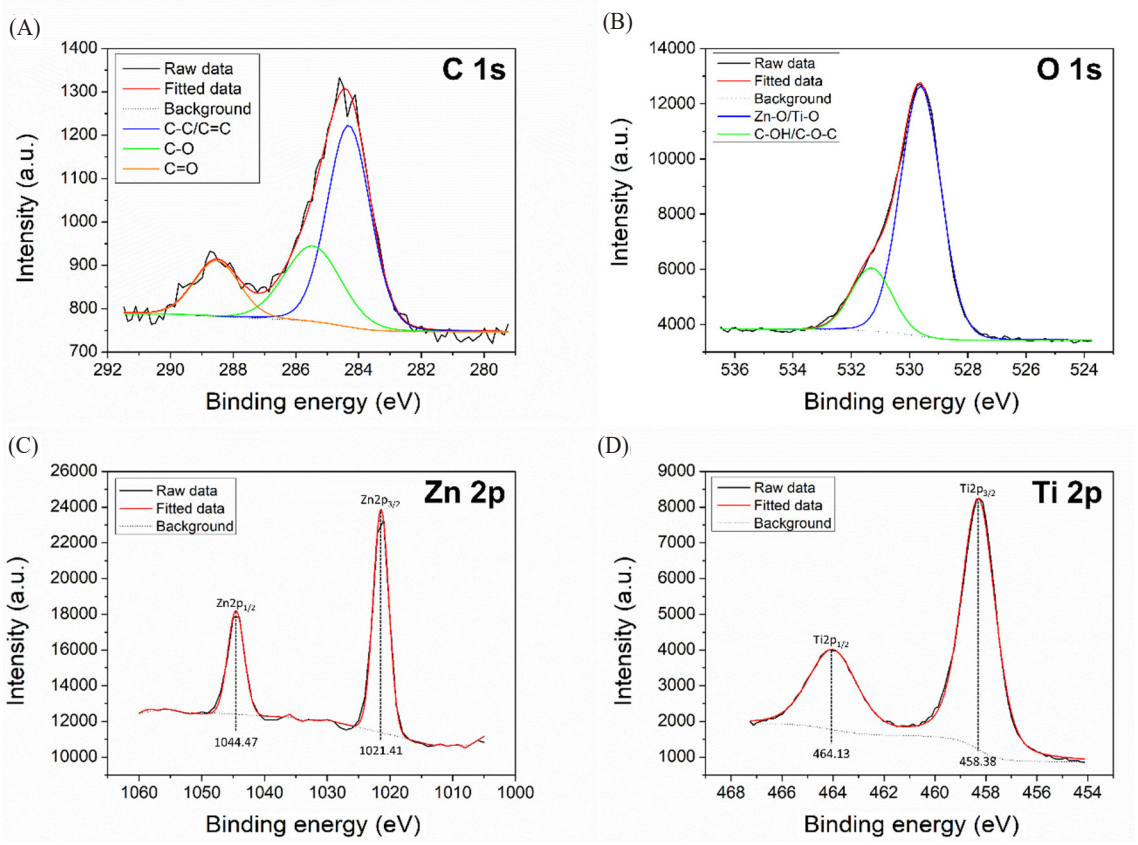

Fig. 7. High-resolution X-ray photoelectron spectroscopy (XPS) spectra of (A) C 1s, (B) O 1s, (C) Zn 2p, and (D) Ti 2p of carbon dot-ZnO-TiO_2 nanocomposite (CDZT).

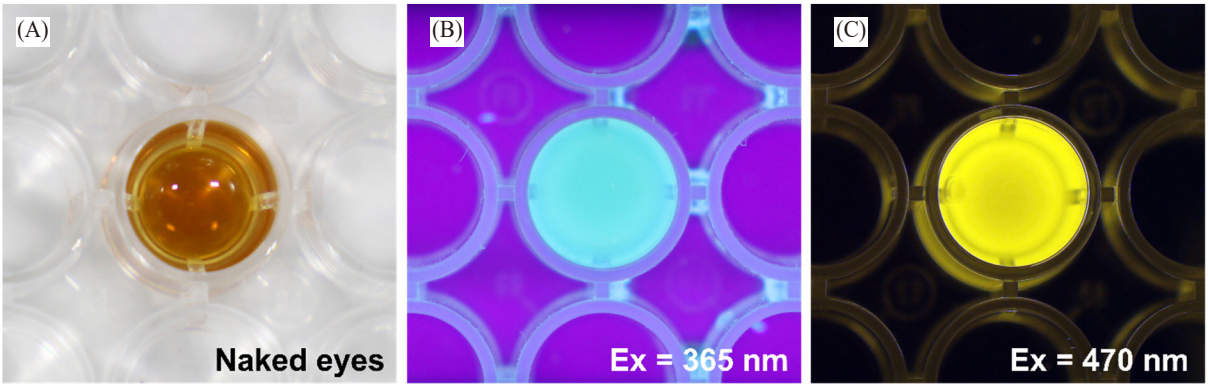

Fig. 8. (A) Photos of the brown-colored carbon dot-ZnO-TiO_2 nanocomposite (CDZT) aqueous solution and (B and C) fluorescence images of CDZT at 365 nm of ultraviolet (UV) light and 470 nm of visible light.

TiO_2, it exhibited excitation-dependent emission characteristics typical of standard CDs (Fig. 9). This behavior indicated that the specificity of the CDs, whose PL properties largely depend on the surface state, was maintained despite the formation of the nanocomposite. Distinct excitation dependence, characterized by the band-to-band transition of an electron from the

https://doi.org/10.47853/FAS.2025.e11

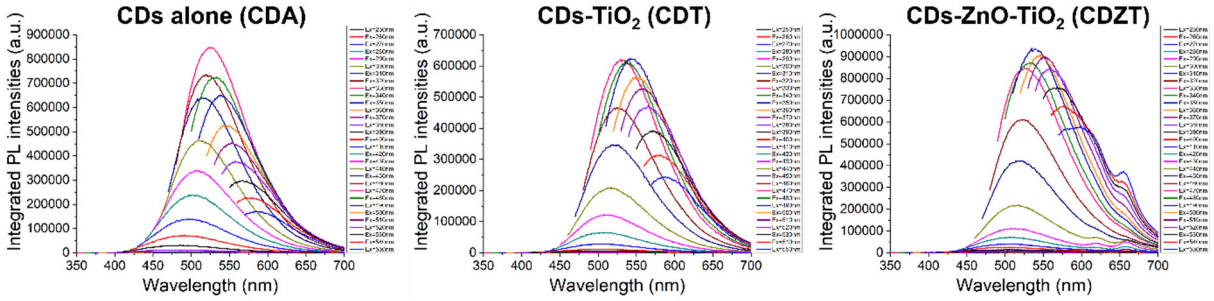

Fig. 9. PL emission spectra of carbon dot alone (CDA), carbon dot–TiO_2 nanocomposite (CDT), and carbon dot-ZnO-TiO_2 nanocomposite (CDZT) with excitation wavelength range from 250 nm to 550 nm and 10 nm increments.

conduction band to the valence band upon photon emission, is induced by defects. These defects result from the trapping of excitons through surface passivation during the carbonization process facilitated by the hydrothermal treatment (Kim et al., 2022b; Sahu et al., 2012).

Compared to that of CDA, the PL spectra of both CDT and CDZT exhibited a slight shift towards longer wavelengths. Furthermore, the PL intensities are higher at an excitation wavelength of 490 nm. In particular, the PL spectrum of CDZT revealed a second peak in the emission wavelength range of 600–700 nm. This peak could be attributed to the formation of a complex between ZnO and TiO_2. The maximum emission was observed at 540 nm under excitation at 490 nm, further highlighting the unique PL properties of the CDZT nanocomposite. For the purpose of this study, two different light sources were employed to excite CDZT, namely UV light at 365 nm and a transilluminator at 470 nm.

The discriminative UV-vis absorption spectra of CDZT, CDA, and CDT are shown in Fig. 10. Among them, CDZT presented a more distinct absorption peak and shoulder peak than the others. CDT exhibited a clear absorption peak with a faint shoulder peak. Although there were differences in the absorption spectra, they showed an absorption peak at approximately 267 nm, assigned to the carbonic core center (Zhang et al., 2021), and a weak shoulder peak at approximately 325–330 nm. The two peaks related to specific types of chemical bonds represent π–π^* transition of C = C bonds of the sp2 domain and n–π^* transition of C = O bonds, respectively. This comprehensive analysis provided significant understaning into the PL properties of the CDZT nanocomposite, contributing to our understanding of its potential applications in various fields.

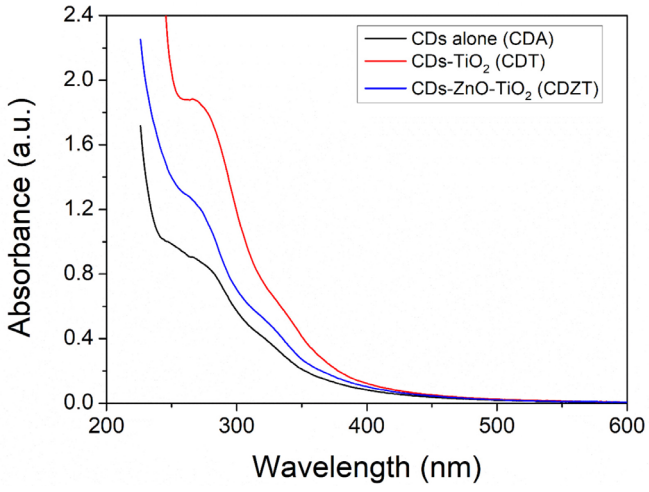

Fig. 10. Ultraviolet (UV)-vis absorption spectra of carbon dot-ZnO-TiO_2 nanocomposite (CDZT).

Antibacterial activity of carbon dot-ZnO-TiO_2 nanocomposite (CDZT) under ultraviolet (UV) and visible light

In this study, we conducted disk diffusion tests to evaluate the antibacterial activity of the CDZT nanocomposite under two different light conditions, namely at 365 nm UV light and 470 nm LED light (Figs. 11 and 12). The as-fabricated CDT was used as a comparative material to benchmark the performance of CDZT (Figs. 13 and 14). The CDZT nanocomposite exhibited distinct differences in antibacterial activity against the four bacterial strains, two gram-negative and two gram-positive, with and without light sources. When exposed to UV light at 365 nm, the inhibition zones were significantly larger, showing an improvement of up to 35%–38% for gram-positive strains than when no light was applied (Table 1). Interestingly, even in

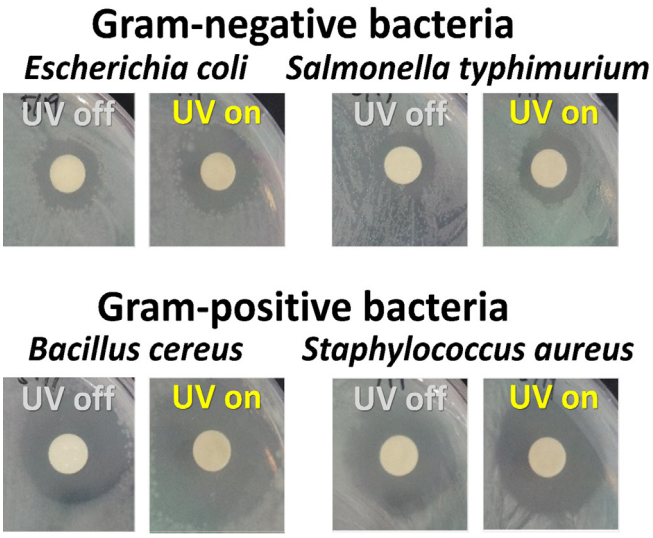

Fig. 11. Photos of the inhibition zones of carbon dot-ZnO-TiO_2 nanocomposite (CDZT) with or without 365 nm of ultraviolet (UV) light.

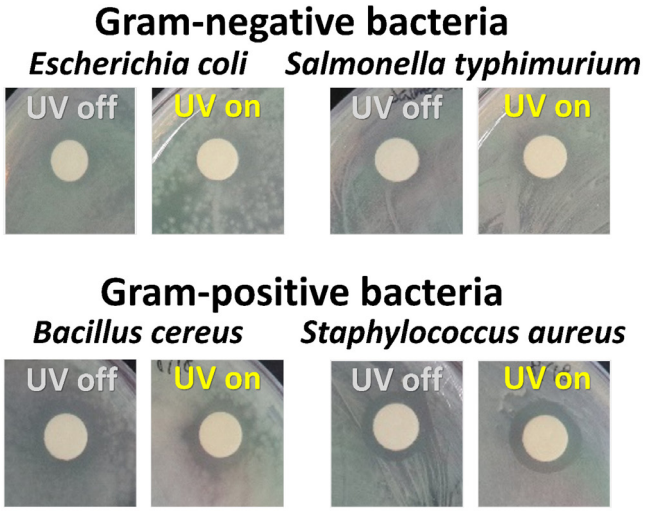

Fig. 13. Photos of the inhibition zones of carbon dot–TiO_2 nanocomposite (CDT) with or without 365 nm of ultraviolet (UV) light.

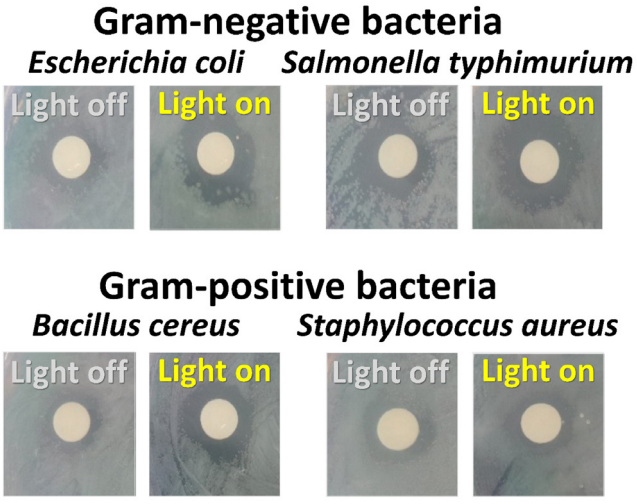

Fig. 12. Photos of the inhibition zones of carbon dot-ZnO-TiO_2 nanocomposite (CDZT) with or without 470 nm of visible light.

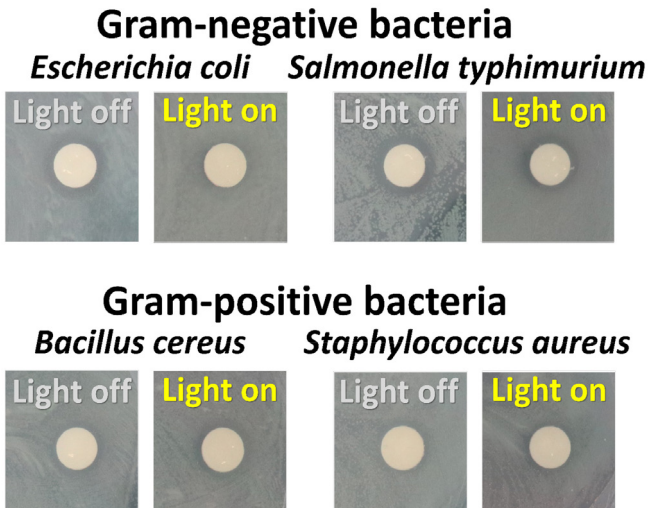

Fig. 14. Photos of the inhibition zones of carbon dot–TiO_2 nanocomposite (CDT) with or without 470 nm of visible light.

the absence of light, a certain degree of inhibition was observed for both gram-negative and gram-positive bacteria. We hypothesized that the inherent antibacterial activity of CDZT was due to the presence of ZnO and TiO2 in the nanocomposite, and that this activity was further enhanced by the CDs upon light irradiation. In comparison, CDT showed no significant inhibition zone against gram-negative bacteria with or without light irradiation, although it showed slightly improved inhibition zones for gram-positive bacteria under UV irradiation.

This suggested that CDT, as a nanocomposite containing TiO_2, also possesses antibacterial activity, which appears to be slightly enhanced under UV irradiation. When compared with

https://doi.org/10.47853/FAS.2025.e11

Table 1. Comparison of the size of inhibition zone for carbon dot-ZnO-TiO_2 nanocomposite (CDZT) against gram-negative and gram-positive bacteria under 365 nm of ultraviolet (UV) light

Bacteria		UV off	UV on (365 nm)	Photo-enhanced antibacterial activity
Gram-negative	*Escherichia coli*	12.87 ± 2.14	14.97 ± 3.95	Yes (16% higher)
	Salmonella typhimurium	11.20 ± 1.66	11.41 ± 1.93	– (1.8% higher)
Gram-positive	*Bacillus cereus*	14.23 ± 5.17	19.60 ± 8.86	Yes (38% higher)
	Staphylococcus aureus	14.77 ± 4.69	19.93 ± 5.35	Yes (35% higher)

our previous research on the antibacterial results using carbon dot-ZnO nanocomposite, the photo-enhanced antibacterial effect of CDZT was significantly improved under the same wavelength of light (Kim et al., 2022b). Under 470 nm light irradiation, CDZT exhibited intriguing antibacterial effects. It showed a high level of antibacterial activity against gram-negative bacteria, unlike the results obtained under UV light. In particular, the antibacterial activity against S. typhimurium improved by more than 50% (Table 2). Another noteworthy observation was related to the irradiation time at 470 nm. Given that the 470 nm light source automatically turned off after 5 min, it is interesting to note that the antibacterial activity significantly increased within the first 5 min of irradiation, as shown in Fig. 12. These findings underscored the possibility of CDZT being a potent antibacterial agent whose activity is modulated by light conditions. Further studies are warranted to fully elucidate the mechanisms underlying these observations and optimize the use of CDZT in antibacterial applications. While CDZT shows great potential, addressing its limitations for incompletely understanding about the exact mechanisms for antibacterial activity as well as in vivo studying to validate these findings in more complex biological systems and exploring future directions will strengthen its impact in antibacterial applications.

Conclusion

S. horneri, a marine alga often considered a nuisance, has been demonstrated in this study as a valuable resource for the fabrication of novel antibacterial nanocomposites. This innovative approach not only utilized an otherwise unusable marine organism but also contributed to the development of advanced antibacterial materials. By generating a CDZT nanocomposite using two precursors and *S. horneri*, we successfully synthesized a light-enhanced antibacterial material. The CDZT nanocomposite exhibited more effective antibacterial activity against gram-positive bacteria under 365 nm UV light and higher antibacterial activity against gram-negative bacteria under 470 nm visible light. Antibacterial nanocomposites could be easily fabricated by a one-pot synthesis method. Furthermore, the precipitate obtained after synthesis could be used individually as pure TiO_2, offering significant advantages in terms of resource circulation and upcycling. The CDZT nanocomposite showed antibacterial activity against both gram-negative and gram-positive bacteria in multiwavelength bands. This included lights commonly used in performance halls, specific exhibition halls, and chambers where plants and fish are raised. Therefore, CDZT nanocomposites derived from *S. horneri* may be highly anticipated to be utilized in various industrial applications. Notably, the CDZT nanocomposite was well-dispersed in water, which further enhanced its potential for industrial use. Additionally, pure TiO_2 was obtained from the residues after synthesis, further demonstrating the efficiency and resourcefulness of this process.

Table 2. Comparison of the size of inhibition zone for carbon dot-ZnO-TiO_2 nanocomposite (CDZT) against gram-negative and gram-positive bacteria under 470 nm of visible light

Bacteria		Light off	Light on (470 nm)	Photo-enhanced antibacterial activity
Gram-negative	*Escherichia coli*	11.37 ± 1.11	15.82 ± 0.61	Yes (39% higher)
	Salmonella typhimurium	11.73 ± 2.32	17.96 ± 0.62	Yes (53% higher)
Gram-positive	*Bacillus cereus*	11.02 ± 0.81	15.55 ± 1.01	Yes (41% higher)
	Staphylococcus aureus	11.91 ± 0.31	12.12 ± 0.91	– (1.7% higher)

Competing interests
No potential conflict of interest relevant to this article was reported.

Funding sources
This work was funded by an in-house project of the National Marine Biodiversity Institute of Korea (MABIK, grant number 2024M00500).

Acknowledgements
A Korean domestic application was filed for the contents described in this study (patent number: 10-2022-0154391).
We would like to thank Kim H.S. for providing some of the *S. horneri* collected from the Buan gun.

Availability of data and materials
Upon reasonable request, the datasets of this study can be available from the corresponding author.

Ethics approval and consent to participate
Not applicable.

ORCID

Kyung Woo Kim	https://orcid.org/0000-0003-0503-9249
Gun-Woo Oh	https://orcid.org/0000-0003-0494-2508
Seok-Chun Ko	https://orcid.org/0000-0002-0509-3336
Ji-Yul Kim	https://orcid.org/0000-0002-9638-7179
Chul Hwan Kim	https://orcid.org/0000-0002-0893-2246
Yong Min Kwon	https://orcid.org/0000-0001-9989-6190
Mi-Jin Yim	https://orcid.org/0000-0002-2086-1823
Moongeun Yoon	https://orcid.org/0000-0002-7125-5460
Dae-Sung Lee	https://orcid.org/0000-0003-0627-1402

References

Aga KW, Efa MT, Beyene TT. Effects of sulfur doping and temperature on the energy bandgap of ZnO nanoparticles and their antibacterial activities. ACS Omega. 2022;7:10796-803.

Azizi-Lalabadi M, Ehsani A, Divband B, Alizadeh-Sani M. Antimicrobial activity of Titanium dioxide and Zinc oxide nanoparticles supported in 4A zeolite and evaluation the morphological characteristic. Sci Rep. 2019;9:17439.

Chahal S, Macairan JR, Yousefi N, Tufenkji N, Naccache R. Green synthesis of carbon dots and their applications. RSC Adv. 2021;11:25354-63.

Cheeseman S, Christofferson AJ, Kariuki R, Cozzolino D, Daeneke T, Crawford RJ, et al. Antimicrobial metal nanomaterials: from passive to stimuli-activated applications. Adv Sci. 2020;7:1902913.

Cho Y, Yamaguchi A, Uehara R, Yasuhara S, Hoshina T, Miyauchi M. Temperature dependence on bandgap of semiconductor photocatalysts. J Chem Phys. 2020;152:231101.

Correa MG, Martínez FB, Vidal CP, Streitt C, Escrig J, de Dicastillo CL. Antimicrobial metal-based nanoparticles: a review on their synthesis, types and antimicrobial action. Beilstein J Nanotechnol. 2020;11:1450-69.

de Oliveira EGL, de Oliveira HP, Gomes ASL. Metal nanoparticles/carbon dots nanocomposites for SERS devices: trends and perspectives. SN Appl Sci. 2020;2:1491.

Faure B, Salazar-Alvarez G, Ahniyaz A, Villaluenga I, Berriozabal G, de Miguel YR, et al. Dispersion and surface functionalization of oxide nanoparticles for transparent photocatalytic and UV-protecting coatings and sunscreens. Sci Technol Adv Mater. 2013;14:023001.

Feng Z, Adolfsson KH, Xu Y, Fang H, Hakkarainen M, Wu M. Carbon dot/polymer nanocomposites: from green synthesis to energy, environmental and biomedical applications. Sustain Mater Technol. 2021;29:e00304.

Gayen B, Palchoudhury S, Chowdhury J. Carbon dots: a mystic star in the world of nanoscience. J Nanomater. 2019;2019:3451307.

Ghirardello M, Ramos-Soriano J, Galan MC. Carbon dots as an emergent class of antimicrobial agents. Nanomaterials. 2021;11:1877.

Haider AJ, Jameel ZN, Al-Hussaini IHM. Review on: titanium dioxide applications. Energy Procedia. 2019;157:17-29.

He S, Meng Y, Liu J, Huang D, Mi Y, Ma R. Recent developments in nanocomposite membranes based on carbon dots. Polymers. 2024;16:1481.

Hochvaldová L, Večeřová R, Kolář M, Prucek R, Kvítek L, Lapčík L, et al. Antibacterial nanomaterials: upcoming hope to overcome antibiotic resistance crisis. Nanotechnol Rev. 2022;11:1115-42.

Huang W, Tao F, Li F, Mortimer M, Guo LH. Antibacterial nanomaterials for environmental and consumer product applications. NanoImpact. 2020;20:100268.

Jia C, Zhang X, Matras-Postolek K, Huang B, Yang P. Z-scheme reduced graphene oxide/TiO_2-bronze/$W_{18}O_{49}$ ternary heterostructure towards efficient full solar-spectrum photoca-

 https://doi.org/10.47853/FAS.2025.e11

talysis. Carbon. 2018;139:415-26.

Jing HH, Bardakci F, Akgöl S, Kusat K, Adnan M, Alam MJ, et al. Green carbon dots: synthesis, characterization, properties and biomedical applications. J Funct Biomater. 2023;14:27.

Kanwal A, Bibi N, Hyder S, Muhammad A, Ren H, Liu J, et al. Recent advances in green carbon dots (2015–2022): synthesis, metal ion sensing, and biological applications. Beilstein J Nanotechnol. 2022;13:1068-107.

Kim KW, Kwon YM, Kim SY, Kim JYH. One-pot synthesis of UV-protective carbon nanodots from sea cauliflower (*Leathesia difformis*). Electron J Biotechnol. 2022a;56:22-30.

Kim KW, Chung D, Jung SH, Kwon YM, Kim JYH, Baek K. Antimicrobial effect of carbon nanodots–ZnO nanocomposite synthesized using *Sargassum horneri*. J Mar Sci Eng. 2022b;10:1546.

Krishnan P, Liu M, Itty PA, Liu Z, Rheinheimer V, Zhang MH, et al. Characterization of photocatalytic TiO_2 powder under varied environments using near ambient pressure X-ray photoelectron spectroscopy. Sci Rep. 2017;7:43298.

Liu J, Li R, Yang B. Carbon dots: a new type of carbon-based nanomaterial with wide applications. ACS Cent Sci. 2020;6:2179-95.

Mendes CR, Dilarri G, Forsan CF, de Sapata VMR, Lopes PRM, de Moraes PB, et al. Antibacterial action and target mechanisms of zinc oxide nanoparticles against bacterial pathogens. Sci Rep. 2022;12:2658.

Nocito G, Calabrese G, Forte S, Petralia S, Puglisi C, Campolo M, et al. Carbon dots as promising tools for cancer diagnosis and therapy. Cancers. 2021;13:1991.

Nocito G, Sciuto EL, Franco D, Nastasi F, Pulvirenti L, Petralia S, et al. Physicochemical characterization and antibacterial properties of carbon dots from two mediterranean olive solid waste cultivars. Nanomaterials. 2022;12:885.

Pei LZ, Wei T, Lin N, Yu HY. Synthesis of zinc oxide and titanium dioxide composite nanorods and their photocatalytic properties. Adv Compos Lett. 2016;25:9-15.

Ribeiro AI, Dias AM, Zille A. Synergistic effects between metal nanoparticles and commercial antimicrobial agents: a review. ACS Appl Nano Mater. 2022;5:3030-64.

Sahu S, Behera B, Maiti TK, Mohapatra S. Simple one-step synthesis of highly luminescent carbon dots from orange juice: application as excellent bio-imaging agents. Chem Commun. 2012;48:8835-7.

Shaker S, Mohsin AK, Edan M. Preparation TiO_2 and ZnO/TiO_2 nanocomposites locally and use against *Staphylococcus aureus*. IOP Conf Ser Mater Sci Eng. 2020;928:072014.

Shameem MM, Sasikanth SM, Annamalai R, Raman RG. A brief review on polymer nanocomposites and its applications. Mater Today Proc. 2021:45;2536-9.

Sindhwani S, Chan WCW. Nanotechnology for modern medicine: next step towards clinical translation. J Intern Med. 2021;290:486-98.

Singh M, Lee KE, Vinayagam R, Kang SG. Antioxidant and antibacterial profiling of pomegranate-pericarp extract functionalized-zinc oxide nanocomposite. Biotechnol Bioprocess Eng. 2021;26:728-37.

Subhan MA, Neogi N, Choudhury KP. Industrial manufacturing applications of zinc oxide nanomaterials: a comprehensive study. Nanomanufacturing. 2022;2:265-91.

Upadhyay GK, Rajput JK, Pathak TK, Kumar V, Purohit LP. Synthesis of ZnO:TiO_2 nanocomposites for photocatalyst application in visible light. Vacuum. 2019;160:154-63.

Wang J, Wang Z, Wang W, Wang Y, Hu X, Liu J, et al. Synthesis, modification and application of titanium dioxide nanoparticles: a review. Nanoscale. 2022;14:6709-34.

Wang W, Lv L, Wang C, Li J. Melamine-assisted thermal activation method for vacancy-rich ZnO: calcination effects on microstructure and photocatalytic properties. Molecules. 2023;28:5329.

Wu X, Abbas K, Yang Y, Li Z, Tedesco AC, Bi H. Photodynamic anti-bacteria by carbon dots and their nano-composites. Pharmaceuticals. 2022;15:487.

Zhang Q, Wang R, Feng B, Zhong X, Ostrikov K. Photoluminescence mechanism of carbon dots: triggering high-color-purity red fluorescence emission through edge amino protonation. Nat Commun. 2021;12:6856.

Zhao WB, Liu KK, Wang Y, Li FK, Guo R, Song SY, et al. Antibacterial carbon dots: mechanisms, design, and applications. Adv Healthc Mater. 2023;12:2300324.